The Astronomical Journal, 158:240 (13pp), 2019 December https://doi.org/10.3847/1538-3881/ab4e16

Gaia 19ajj: A Young Star Brightening Due to Enhanced Accretion and Reduced Extinction

Lynne A. Hillenbrand[1], Bo Reipurth[2], Michael Connelley[2], Roc M. Cutri[3], and Howard Isaacson[4,5]
[1] Department of Astronomy, California Institute of Technology, Pasadena CA 91125, USA; lah@astro.caltech.edu
[2] Institute for Astronomy, University of Hawaii at Manoa, 640 N. Aohoku Place, Hilo, HI 96720, USA
[3] IPAC, California Institute of Technology, Pasadena CA 91125, USA
[4] Astronomy Department, University of California, Berkeley, CA 94720, USA
[5] University of Southern Queensland, Toowoomba, QLD 4350, Australia
Received 2019 July 16; revised 2019 October 12; accepted 2019 October 14; published 2019 November 20

Abstract

We report on the source Gaia 19ajj, identifying it as a young star associated with a little-studied star-forming region seen along a complex line of sight through the Gum Nebula. The optical lightcurve recently recorded by *Gaia* exhibits a slow and unsteady 5.5 mag rise over about 3 yr, while the mid-infrared lightcurve from NEOWISE over the same time period shows a 1.2 mag rise having similar structure. Available color information is inconsistent with pure extinction reduction as the cause for the photometric brightening. Optical spectroscopic characteristics in the current bright phase include: little in the way of absorption except for the hallmark Li I 6707 Å signature of youth plus weak, e.g., Ca I and notably Ba II; strong wind/outflow in Ca II, Mg I b, Na I D, Hα, K I, and O I; jet signatures in [O I], [S II], [Ca II], [Fe II], and [Ni II]; and narrow rest-velocity emission in neutral species such as Fe I, Ni I, and Mg I. The infrared spectrum is also characterized by outflow and emission, including: a hot He I wind, jet lines such as [Fe II] and H_2; and weak narrow rest-velocity atomic line emission. The ^{12}CO bandheads are weakly in emission, but there is also broad H_2O absorption. Gaia 19ajj exhibited a previous bright state in the 2010–2012 time frame. The body of photometric and spectroscopic evidence suggests that the source bears resemblance to V2492 Cyg (PTF 10nvg) and PV Cep, both of which similarly experience bright phases that recur on long timescales, with large-amplitude photometric variations and emission-dominated spectra. We interpret the behavior of Gaia 19ajj as caused by cycles of enhanced disk accretion accompanied by reduced extinction.

Unified Astronomy Thesaurus concepts: Stellar accretion disks (1579); Stellar accretion (1578); Circumstellar matter (241); Stellar activity (1580); Star formation (1569); T Tauri stars (1681); Herbig Ae/Be stars (723)

1. Introduction

The evolution of circumstellar material around young stars is a topic of great interest for problems ranging from the build-up of stellar mass during star formation and early stellar evolution to the formation of planets in circumstellar disks. These processes are heavily influenced over the first several mega-years of a star's life by the trades between—on the one hand—envelope infall and disk accretion bringing mass inward, and—on the other hand —outflows, jets, and winds arising from a range of locations in the stellar/circumstellar environment, which eject mass from the system.

One way of tracing dynamical effects in young stars is through photometric variability. For nearly a century, highly variable astronomical objects have been reported in the literature (e.g., Joy 1945; Herbig 1946) that were later associated with young stars (Ambartsumian 1949; Herbig 1954, 1957). The many flavors of young star variability were subsequently characterized by various authors, notably by Herbst et al. (1994) and Herbst & Shevchenko (1999); see also Ismailov (2005). Over the past decade, the true diversity of young star behavior in the time domain has become more fully appreciated and the lightcurve categories more rigorously defined. Increasingly higher cadence and more photometrically precise data sets (e.g., Cody et al. 2014; Cody & Hillenbrand 2018), as well as long-duration, multidecade investigations (e.g., Ibryamov et al. 2015; Mutafov et al. 2019) have contributed. Such studies have been possible due to dedicated monitoring efforts over small fields, and modern all-hemisphere, and even all-sky, time domain surveys. The involvement of amateur astronomers with sophisticated equipment and eyes on the sky has also been important, particularly in the identification of rare large-amplitude brightness changes.

For nearly a half century, we have recognized a small sample of large and very large-amplitude (>3 mag) young star variables as outbursting sources (Herbig 1977, 1989; Connelley & Reipurth 2018). The basic paradigm of episodic accretion, or punctuated periods of enhanced mass accretion/outflow that builds up the final ~10% of the stellar mass, was developed based on these early but scant observations (see a review by Hartmann & Kenyon 1996). The rates for the different types of outbursts remain relatively poorly constrained empirically (Hillenbrand & Findeisen 2015), though for recent significant progress see Contreras Peña et al. (2019). Especially over the past decade, our understanding of the diversity in behavior of young stars during such large-amplitude brightenings has been enhanced by the coordination of multicolor photometric and multiwavelength spectroscopic follow-up of detected brightening events.

In this paper, we describe a large-amplitude brightening of the newly appreciated young stellar object Gaia 19ajj. The *Gaia* mission, although primarily an astrometric mission, offers public alerts[6] based on photometric changes exceeding 2 mag in the broadband optical G filter (Hodgkin et al. 2013, 2020, in preparation). One such alert was issued on 2019 January 31 for Gaia 19ajj. Since that time, the source at position 08:10:45.78–36:04:30.94 (J2000.) has continued to brighten.

[6] *Gaia* Alerts; http://gsaweb.ast.cam.ac.uk/alerts.

In this paper, we first describe the source Gaia 19ajj and its environment in Section 2. In Section 3, we report on the publicly available *Gaia* lightcurve of Gaia 19ajj and its historical context based on the All-Sky Automated Survey (ASAS) and VST Photometric Hα Survey (VPHaS) photometry. We also present *Wide-field Infrared Survey Explorer* (*WISE*) and NEOWISE photometry at mid-infrared wavelengths covering essentially the same time baseline. Our follow-up near-infrared photometry is presented in Section 4 and the critical spectroscopy at both optical and infrared wavelengths in Section 5. Section 6 contains a summary and short discussion of the context of this source amid the complex zoo of young star variables, and Section 7 contains our conclusions regarding its similarity to sources like V2492 Cyg (PTF 10nvg; Covey et al. 2011; Hillenbrand et al. 2013; Giannini et al. 2018) with PV Cep another good analog.

2. The Source

2.1. Environment

Gaia 19ajj is located within an optically opaque small cloud, positioned about 1°.5 below the southern galactic plane. Figure 1 shows the large-scale region. The sightline passes the northern part of the Vela Molecular Ridge, broadly located toward the Gum Nebula. The best known objects in this general area are the CG 30/31 globules containing HH 120, located 15′ to the west (Reipurth 1983). About a degree to the northeast is the prominent H II region RCW 19 = Gum 10 (Gum 1955; Rodgers et al. 1960).

Between these two features is a small cloud, Dobashi 5180 (Dobashi 2011), in which Gaia 19ajj is located. Other very nearby cataloged structures include the dark clouds DC 253.6-1.3 (Hartley et al. 1986) and G253.56-1.32 (Dutra & Bica 2002), and the Planck-identified dust clump and dense core PLCKECC G253.49-01.26 (Planck Collaboration et al. 2011) to the east. The Gaia 19ajj position is just southeast of IRAS 08088-3554 which is identified as a compact H II region.

The immediate region of Gaia 19ajj features many diffuse objects in optical images from the National Optical Astronomy Observatory (NOAO) DECam Plane Survey (DECaPS; Schlafly et al. 2018), and there is evidence of a grouping of bright red stars, including Gaia 19ajj, in the mid-infrared *WISE* images. The local cloud is clearly a recently active star-forming region. The most well-studied young star in the vicinity is HBC 556, a few arcmin to the west. Pettersson (1987a, 1987b) identified this source as PHα21, of spectral type M4, in a broad-area search for Hα emission stars in the region between the cometary globules and RCW 19. In order to gauge the level of star formation activity in this region, we looked for the presence of additional Hα emission sources in the vicinity of Gaia 19ajj by examining an Hα image obtained as part of the AAO SuperCOSMOS survey (Parker et al. 2005). We identify four such sources in Figure 1. A color image from DECam (available via the ALADIN service) shows even more detail of these and additional, fainter nebulae in the vicinity.

2.2. Distance

The *Gaia* DR2 (Gaia Collaboration et al. 2018) distance to Gaia 19ajj, derived by simply inverting the measured parallax (1.200 ± 0.201 mas), is 832^{+170}_{-120} pc. This can be compared to previous estimates of distance in this region of sky. First, Westerlund (1963) discovered an OB association, which he called Puppis OB III, apparently related to the RCW 19 H II region to the east of Gaia 19ajj, and estimated its distance at around 1700 pc. Considering the more proximately located HBC 556, Pettersson (1987a) assumed that this star is located within the Gum Nebula, at the same approximate distance of the cometary globules to the west of Gaia 19ajj, estimated at around 450 pc. We concur that from its brightness and spectral type, HBC 556 cannot be a distant object. Finally, a kinematic distance of 3.3 kpc was suggested by Bhatt et al. (1998) for the associated small cloud itself, but this value is both highly uncertain and improbable given the other evidence. We adopt the 832 pc distance from *Gaia* DR2. This implies that Gaia 19ajj, and thus presumably the Dobashi 5180 small cloud, are located behind the Gum Nebula.

2.3. Spectral Energy Distribution

The spectral energy distribution (SED) that can be assembled for Gaia 19ajj (Figure 2; see also the Vizier version[7]) rises from 0.5 to 4 μm, then turns over with flat or only slightly declining energy out to 24 μm. The SED is comprised of photometry taken at different epochs—when the source was in various photometric states. Catalog data originates from the The Naval Observatory Merged Astrometric Dataset (NOMAD; Zacharias et al. 2005), USNO-B (Monet et al. 2003), VPHaS DR2 (Drew et al. 2014), Gaia DR2 (Gaia Collaboration et al. 2018), Two Micron All Sky Survey (2MASS; Cutri et al. 2003; Skrutskie et al. 2006), Deep Near Infrared Survey of the southern sky (DENIS),[8] *WISE* (Wright et al. 2010), *Midcourse Space Experiment* (*MSX*; Price et al. 2001), and *AKARI* (Ishihara et al. 2010) catalogs. The *G*, *BP*, *RP* photometry from *Gaia* DR2 is an order of magnitude fainter than the somewhat earlier VPHaS optical photometry and much fainter than the decades earlier USNO-B value (see Figure 3).

Regardless of the demonstrated short-wavelength photometric variability, Gaia 19ajj is clearly a "Class I" type young stellar object with a flat mid-infrared SED.[9] This SED category is associated with disk+envelope circumstellar geometry, suggesting a significant amount of high latitude material above the disk that is distributed in a more spherical-like geometry, with ongoing infall and rapid accretion onto the central stellar object. We do not attempt to model the SED given the demonstrated variability and the geometric complications for the radiative transfer.

The SED also implies that at least some of the short-wavelength light may be scattered rather than direct. This is consistent with the fact that the fainter-state photometry represented in the *Gaia* DR2 data does not demand significantly higher reddening relative to the much brighter state of the VPHaS measurements. As discussed below, the photometric changes in Gaia 19ajj are likely not explained by extinction changes alone.

2.4. Other Available Information

There are no previous publications studying this specific star (2MASS 08104579-3604310), though it does appear based on

[7] http://vizier.u-strasbg.fr/vizier/sed/?submitSimbad=Search&-c=08:10:45.78%2B-36:04:30.94&-c.r=2&-c.u=arcsec

[8] http://cdsweb.u-strasbg.fr/denis.html

[9] Quantitatively, we measure a spectral index from the 2MASS K_s band and *WISE* 22 μm band photometry as +0.36.

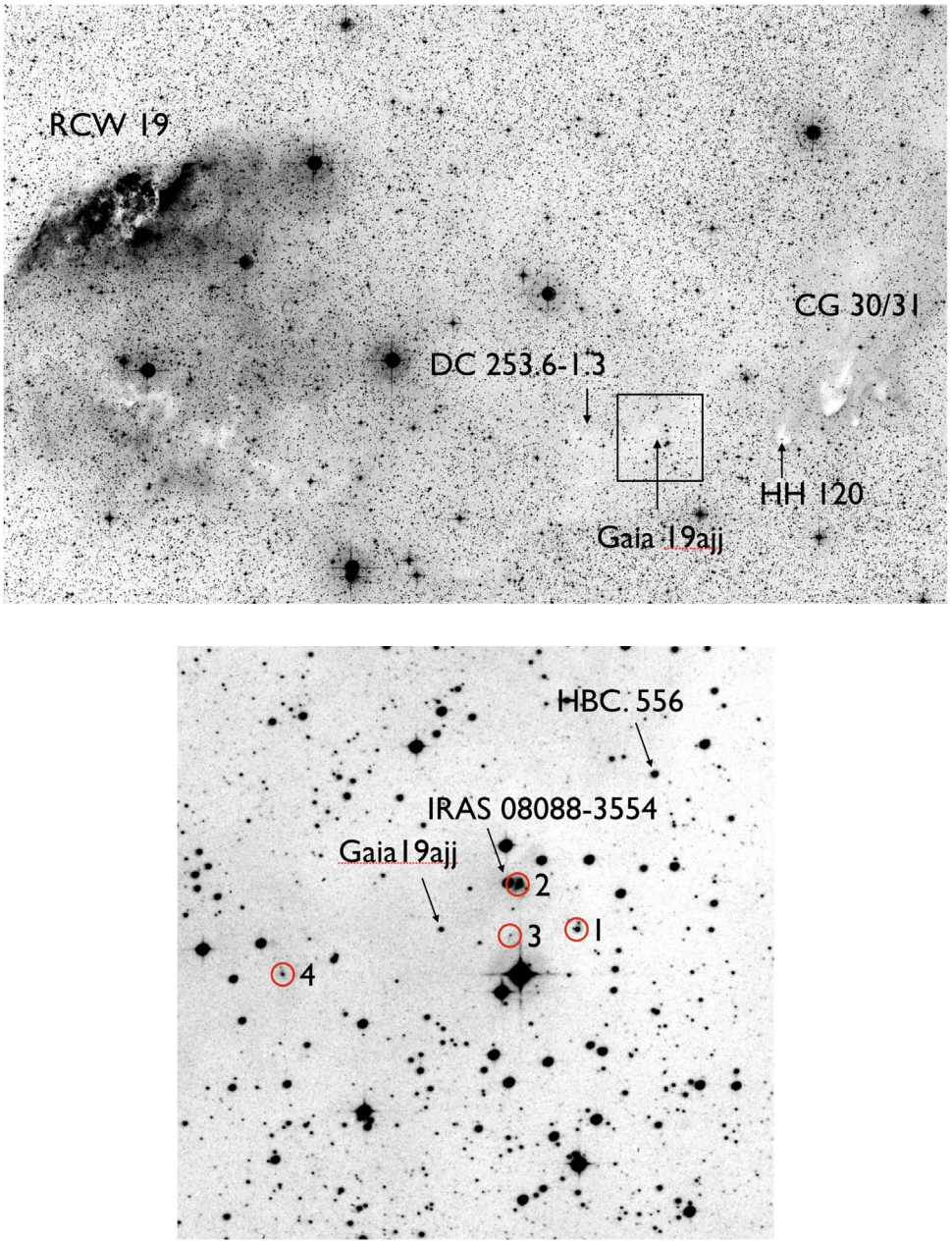

Figure 1. Top: Anglo-Australian Observatory (AAO) red Schmidt plate from the Second Epoch Survey (SES) over 2° × 1° showing the general region. Gaia 19ajj is located in a small dark cloud to the southeast of the CG 30/31 complex. The box indicates the area shown in the bottom panel. Bottom: United Kingdom Survey Telescope (UKST) SuperCOSMOS Hα image over 10′ × 10′ highlighting the location of Gaia 19ajj. Newly identified compact emission nebulae are numbered as are various objects discussed in the text. The image orientation is standard, with north upwards and east leftwards, to within 1°–2° over the wide field.

its *WISE* colors in the large catalog of Marton et al. (2016) identifying candidate young stellar objects.

Gaia 19ajj is an apparent Hα emitter, even in previously fainter states. The VPHaS catalog (Drew et al. 2014) provides a brightness of $r = 16.86$ mag and a moderate $r - i$ color of 1.13 ± 0.02 mag, along with an emission index of $r - \mathrm{H}\alpha = 0.89 \pm 0.02$ mag. According to the models in Figure 2 of Barentsen et al. (2013), the source would be an obvious Hα emitter, with an equivalent width of several tens of Angstroms.

Given the SED, as well as the large-amplitude photometric variability described below, it is unwise to attempt a luminosity calculation. However, the observed optical colors suggest a spectral type earlier than $\sim M3$, assuming there is also some color contribution from reddening. Adopting the ≈830 pc distance, the absolute magnitude in an average part of the lightcurve (see below) is $M_r = 7.26 - A_r$, where A_r is the unknown value of the extinction in the r-band. A typical luminosity around 1 $L_\odot$ for a young pre-main-sequence star would suggest $A_r \approx 3$ mag.

3. The Lightcurve

3.1. Optical

Figure 3 shows the *Gaia* G-band lightcurve[10] with the last update for our analysis occurring on 2019 February 28. No

[10] http://gsaweb.ast.cam.ac.uk/alerts/alert/Gaia19ajj/

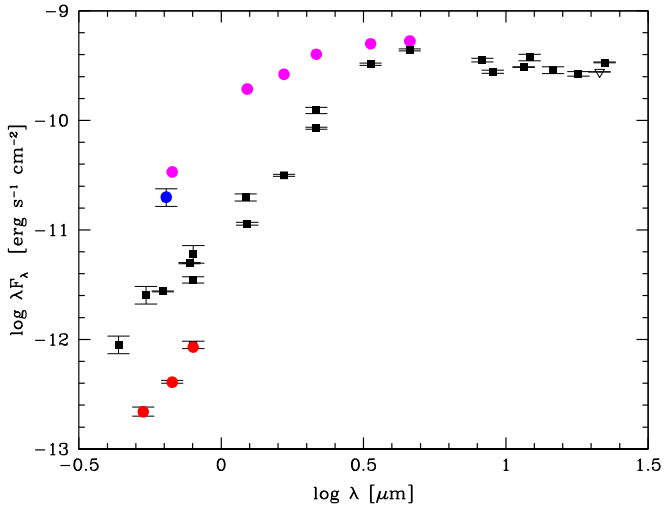

Figure 2. Non-simultaneous SED of Gaia 19ajj. Historical photometric variability of the source is apparent in a notably brighter photographic plate measurement (blue) and the notably fainter *Gaia* DR2 magnitudes (red), relative to the other recorded optical data points that define a reasonably consistent SED. Recent data from *Gaia*, IRTF, and NEOWISE (magenta) are brighter and bluer than any previously recorded measurements. The SED indicates a "Class I" young stellar object type.

error estimates are provided but we adopt 0.05 mag uncertainty. We include an VPHaS (Drew et al. 2014) *r*-band measurement that has been approximately converted to the *Gaia* photometric system (using the procedure described in Hillenbrand et al. 2018). Also shown is the *V*-band and *g*-band data available from ASAS (Shappee et al. 2014). These data have higher cadence than the *Gaia* data, and indicate quasiperiodic oscillations during the 2018–2019 rise, with a periodogram peak around 24 days. We investigated the availability of *Transiting Exoplanet Survey Satellite* (*TESS*) data for this source, which was observed from 2019 January 7 through February 28, but the *TESS* pixels are too big given the field density for a viable lightcurve to be derived at the current level of *TESS* data processing.

The total brightening of Gaia 19ajj over the past three years exceeds 5.5 mag in the *Gaia G*-band. While impressive, and possibly suggestive of an outbursting source such as an FU Ori star, Gaia 19ajj was also bright in early 2012, conceivably as bright as it is now. The subsequent large-amplitude fade and more recent re-brightening at both infrared and optical wavelengths suggests that the photometric excursions may have a complex interpretation, such as being due in part to accretion variations and in part to extinction variations. A long-duration color time series would help in the assessment. Unfortunately, there is little optical color information available at present. By matching the time series between *Gaia* and ASAS, we derive only a crude $g - G$ color estimate in the range of 1.2–1.8 mag and no meaningful color variability information.

The historical record of photographic plate measurements of Gaia 19ajj supports repeated large-amplitude brightening and fading. The USNO-A2 (Monet 1998) records $R = 17.25$ mag for a mean epoch between blue and red observations of 1978.5, while the USNO-B1 (Monet et al. 2003) gives $R = 14.66$ mag for mean epoch 1982.3. In other words, the source has exhibited approximately 3 mag variability on few year timescales in the past, similar to what has occurred over the past 4–7 yr.

3.2. Infrared

Variability is also evident in mid-infrared lightcurves. Gaia 19ajj is well detected in data from both the primary *WISE* mission (Wright et al. 2010) and the NEOWISE Reactivation mission (Mainzer et al. 2014).

The 3.4 and 4.6 μm (*W1* and W2) profile-fit photometry for Gaia 19ajj was drawn from the *WISE* All-Sky, 3-Band Cryo, Post-Cryo, and NEOWISE Reactivation Single-exposure Source Databases. Measurements were used only from exposures for which the image quality parameter *qual_frame* was greater than zero, and on which the source lies more than 50 pixels from the image edge. Gaia 19ajj is formally saturated in all *WISE*/NEOWISE images, requiring additional attention in order to present quality photometry. Specifically, the profile-fit photometry of saturated sources exhibits a flux-dependent bias of varying degrees. Therefore, we derived and applied corrections, now published,[11] to the source database magnitudes in order to compensate for the photometric bias.

The median values of the corrected *W1* and *W2* magnitudes for each observation epoch were computed. The uncertainties associated with each median magnitude are the standard deviation of the population of the corrected magnitudes within each epoch. These values are typically slightly smaller than the median of the uncertainties (error) of the individual corrected magnitudes that include the contribution of the systematic uncertainties of the photometric bias corrections. *WISE/NEOWISE* photometry is provided in Table 1.

As illustrated in Figure 3, the *WISE* data points from 2010 are relatively bright, while NEOWISE measured fading between 2014 May and November, then gradual brightening from about MJD $\approx$ 57,000 to the present. There is superposed variability that generally traces the pattern of the optical fluctuations, but at lower amplitude. The cumulative brightening since 2014 November is about 1.2 mag in *W1* (3.6 μm) compared to >5 mag in *G* (0.67 μm).

Figure 4 shows the *WISE/NEOWISE* color curve which indicates that the source has been getting gradually bluer since about MJD $\approx$ 57,000, while it has become brighter (Figure 3). Figure 4 also shows that there is a direct and tight correlation between color and magnitude. However, a least-squares fit indicates that the magnitude–color slope is relatively shallow at $W1 = 2.39 \times (W1 - W2) + 4.29$ with rms = 0.10 mag. This can be compared to the slope of 4.31 expected for interstellar extinction (Indebetouw et al. 2005, adopting the Spitzer extinction law as approximately correct for the *WISE* bands). If interpreted as extinction, the total color change would correspond to $A_V = \Delta(W1 - W2)/(0.56 - 0.43) \times 8.8 = 67.7 \times \Delta(W1 - W2) \approx 35$ mag. However, there is more color change than expected given the magnitude change, which suggests that at least some of the blueing behavior is intrinsic to the source and not just extinction clearing.

This shallow color slope is also apparent in the near-infrared. As discussed below, comparing the changes in $J - H$ versus $H - K$ between 2MASS and new Infrared Telescope Facility (IRTF) photometry shows larger $H - K$ change relative to $J - H$ than would be expected under standard interstellar reddening assumptions. As noted above, the SED also shows an inconsistency between the large change in optical brightness relative to only a small change in optical color.

[11] Section II.1.c.iv.a of the Explanatory Supplement to the NEOWISE Data Release Products (Cutri et al. 2015).

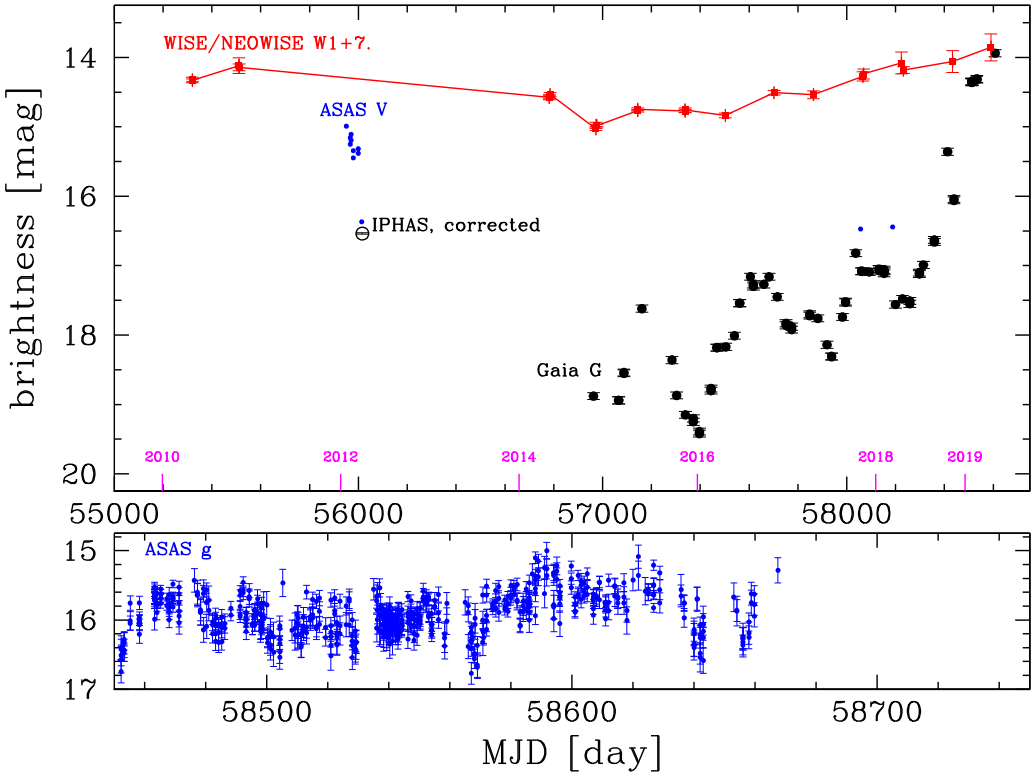

Figure 3. Top panel: available lightcurve data for Gaia 19ajj between 2010 and 2019. Black symbols are the *Gaia G*-band (effective wavelength 0.673 μm) with assumed 0.05 mag error bars, plus an *VPHaS r*-band measurement converted to *G*-band. Blue points are from ASAS and measured in *V*-band (*g*-band data points are shown in the bottom panel). Gaia 19ajj has brightened optically by over 5 mag during the past three years, but was also bright in the 2010–2012 time frame. Red points are *WISE* and NEOWISE measurements at 3.4 μm, shifted downward by 6.75 mag in order to compare to the optical. The mid-infrared also shows recent long-term brightening, exceeding 1 mag over the past three years. Bottom panel: zoom-in to the latest epochs of ASAS data, all in the *g*-band. Short timescale variability accompanies a plateau phase of the recent overall brightening episode; the oscillations occur on a timescale of several weeks. Vertical lines indicate the epochs of field coverage by *TESS* at the high cadence (see the text).

Table 1
WISE and NEOWISE Measurements of Gaia 19ajj

MJD [day]	σ(MJD) [day]	*W1* [mag]	σ(W1) [mag]	Error(W1) [mag]	*W2* [mag]	σ(W2) [mag]	Error(W2) [mag]
55320.08	0.404	7.324	0.031	0.051	6.044	0.025	0.066
55511.16	0.363	7.131	0.047	0.086	5.950	0.057	0.107
56782.13	0.351	7.577	0.028	0.058	6.237	0.073	0.101
56785.19	0.316	7.533	0.025	0.062	6.243	0.055	0.102
56973.14	0.361	7.981	0.044	0.036	6.415	0.028	0.084
56976.18	0.279	7.982	0.016	0.036	6.414	0.037	0.083
57143.97	0.387	7.760	0.019	0.043	6.360	0.044	0.085
57337.97	0.347	7.759	0.025	0.044	6.294	0.047	0.097
57502.94	0.301	7.836	0.027	0.041	6.414	0.045	0.083
57702.24	0.376	7.508	0.028	0.065	6.214	0.068	0.104
57863.50	0.342	7.538	0.046	0.062	6.172	0.092	0.107
58066.31	0.343	7.274	0.065	0.096	6.021	0.118	0.117
58069.14	0.365	7.237	0.065	0.103	5.982	0.093	0.117
58223.95	0.327	7.086	0.119	0.127	5.857	0.122	0.126
58232.40	0.016	7.200	0.017	0.110	5.894	0.005	0.122
58433.38	0.329	7.062	0.152	0.127	5.849	0.117	0.126
58590.92	0.313	6.851	0.171	0.127	5.811	0.111	0.131

Note. MJD = mean Modified Julian Date. W1,W2 = median *WISE* 3.4 and 4.6 μm bias-corrected photometric measurements. σ = dispersion in values. error = median of bias-corrected asymmetric uncertainties.

3.3. Lightcurve Assessment

Both the *Gaia* lightcurve and the NEOWISE lightcurve exhibited quasiperiodic behavior over the few years prior to the recent steep optical rise. Then, starting in early 2018 and continuing into 2019, the slope changed and Gaia 19ajj brightened by another several magnitudes ($\sim$3.5 in the optical and $\sim$1 in the infrared). The optical slope was -0.31 mag/month over about 10 months.

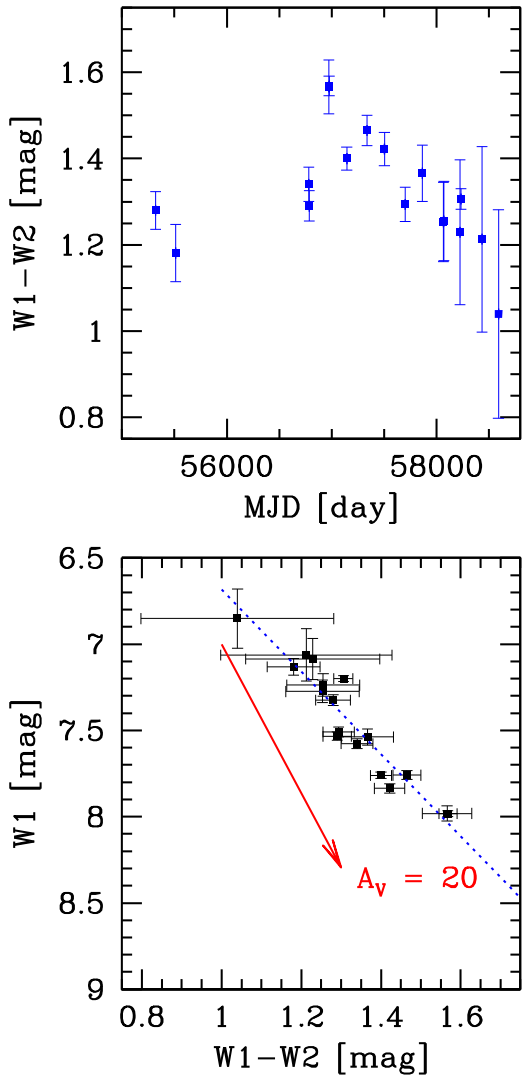

Figure 4. Top panel: *WISE*/NEOWISE color evolution between 2010 and 2018 showing the blueing of the source during the photometric rise illustrated in Figure 3. Note that the source was also relatively blue in 2010, albeit still red in an absolute sense, which we ascribe as due to circumstellar dust. Bottom panel: color–magnitude diagram in *WISE*/NEOWISE filters. A linear fit to the data (blue line) demonstrates the distinction of the color–magnitude behavior of Gaia 19ajj from the expectations for extinction and reddening (red vector).

The optical and mid-infrared lightcurve evidence for wavelength-dependent, long-term photometric brightening that is punctuated by brief fading events suggests that extinction variability may be an important consideration in interpreting the behavior of Gaia 19ajj. However, extinction variations are not the entire story. Accretion variability is driving some of the brightening and blueing, which also has the effect of reducing the amount of dust, and thereby diminishing the line-of-sight extinction. This is the same interpretation as is invoked for several better-studied sources with well-characterized large-amplitude and long-timescale lightcurves, like V2492 Cyg and PV Cep (see the discussion in Section 6).

4. New Infrared Photometry

Gaia 19ajj was observed in *JHKL′* bands on the night of 2019 February 3 (UT) using the slit viewing camera of SpeX (Rayner et al. 2003) at the NASA Infrared Telescope Facility. Conditions were photometric and the source was observed at an airmass of 1.85 resulting in FWHM = 0.″92, which is sampled at 0.″12 pixel^{-1}. The filters in SpeX are in the MKO photometric system (Simons & Tokunaga 2002). We observed UKIRT faint standard FS 123 for the JHK flux calibration, and HD 84800 for the L' flux calibration. For each image, we subtracted off a dark then divided by a normalized sky flat. We then subtracted the median sky value from each image, and aligned and coadded the frames together. Aperture photometry was done with *imexam* in IRAF using a target aperture radius of 20, 23, and 26 pixels, a buffer of 10 pixels, and a sky annulus 10 pixels wide. Since the non-destructive reads and coadds are added together in IRTF data, we were careful to divide by the value of the DIVISOR header keyword. The resulting magnitudes were corrected for airmass using the extinction coefficients for Maunakea in Krisciunas et al. (1987).

The resulting measurements are $J = 10.749$; $H = 9.634$; $K = 8.406$; $L' = 7.135$. The formal errors are about 0.01 mag, but the real errors are dominated by the systematics of the airmass correction, and thus larger than this.

Transformation to the 2MASS photometric system can be achieved using the equations in Connelley et al. (2007). Relative to the JHK photometry reported in the 2MASS catalog (Cutri et al. 2003), the recently measured colors of Gaia 19ajj are bluer in a manner that might indicate motion roughly along a reddening vector, with a reduction in A_V of about 6 mag suggested. However, there is more $H - K$ difference relative to the $J - H$ difference than expected. Some of the blueing color could be caused by accretion effects rather than reduction in extinction, similar to our interpretation of the *WISE*/NEOWISE color changes.

5. New Infrared and Optical Spectroscopy

5.1. Observations

We obtained near-infrared spectra using the IRTF and SpeX (Rayner et al. 2003) on 2019 February 3 (UT) in both short wavelength cross-dispersed (SXD; 0.7–2.4 μm) and long wavelength cross-dispersed (LXD; 1.7–4.2 μm) modes. The resolution with the 0.″5 slit was $R \approx 1200$. For the SXD data the realized signal-to-noise ratio (S/N) per exposure is ∼80 in the *Y*-band and ∼300 in the *K*-band (with 10 exposures taken for 30 minutes of total exposure time). For the LXD data the S/N is ∼50 per exposure in L' (with 16 exposures taken for 8 minutes of total exposure time). The *K*-band seeing was about 0.″5 at zenith but closer to 1″ for observations taken over 1.78 to 1.95 airmasses at the target position. A second SXD spectrum was obtained on 2019 March 26 (UT) under somewhat worse seeing conditions. All data were reduced with SpeXtool (Cushing et al. 2004). In addition to the spectroscopy, a small set of H_2 and broadband *K* images were obtained on the March 26 observing date, and show spatially extended H_2 emanating from the southeast (despite the poor seeing of ∼1.″9), extending to about 7″.

We obtained an optical echelle spectrum between ∼3400–7900 Å at a resolution of $R \approx 60{,}000$ using the Keck I telescope and High Resolution Echelle Spectrometer (HIRES; Vogt et al. 1994) on 2019 February 14 (UT). Data acquisition used the standard operating procedures of the California Planet Search described in Howard et al. (2010). Under temporarily clear skies and ∼2.″0 seeing, a 1500 s exposure resulted in a spectrum with S/N = 15 at 5500 Å. We aligned the Li I

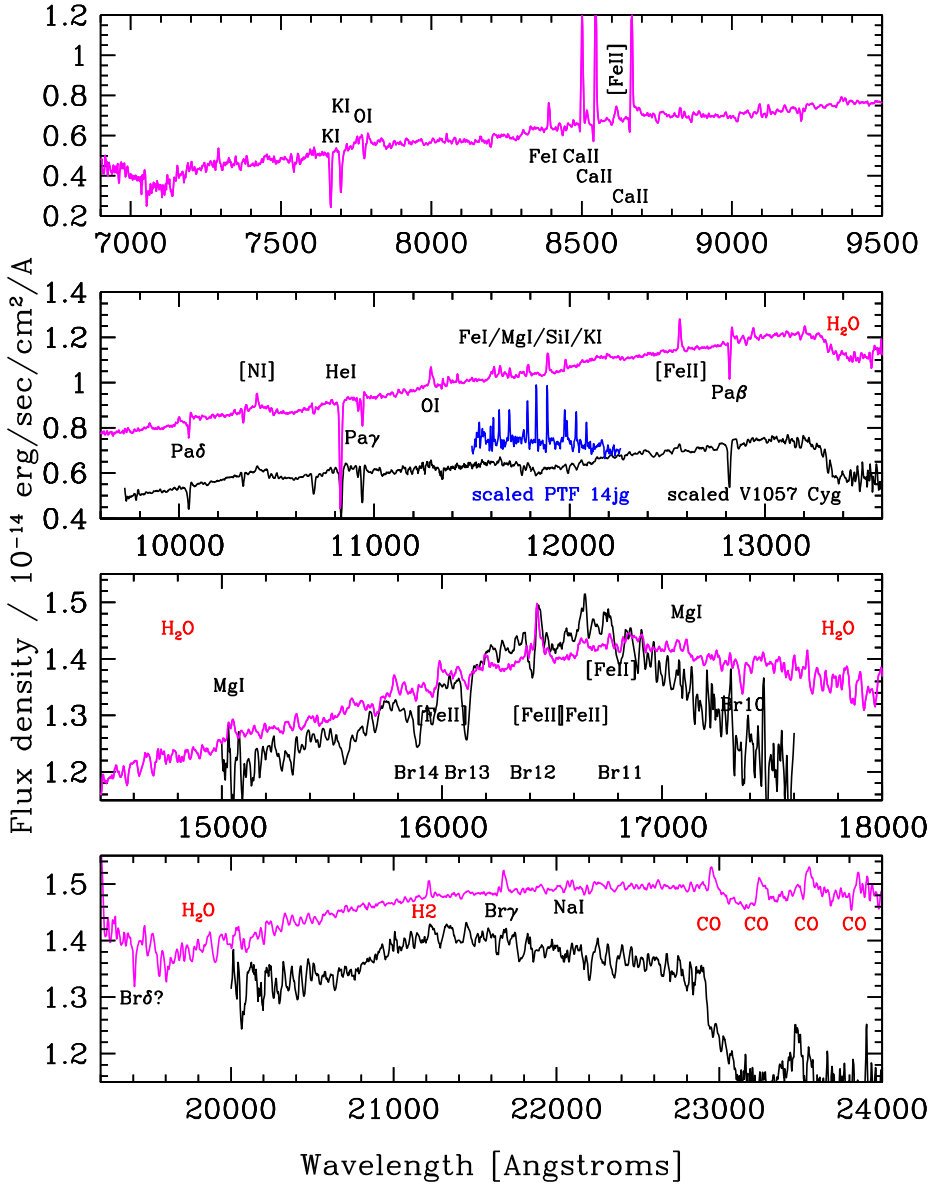

Figure 5. IRTF/SpeX spectrum of Gaia 19ajj in magenta compared with a Palomar/TripleSpec spectrum of V1057 Cyg in black, showing similarity in the overall spectral shape and broad absorption, and with a snippet of the spectrum of PTF 14jg in blue, showing similar but stronger emission in the *J*-band. Various permitted and forbidden atomic lines are labeled (black), as are molecular lines and broad bands (red).

absorption feature to determine a source radial velocity of $+35.8$ km s^{-1}.

Finally, we obtained an infrared echelle spectrum in the 1 μm *Y*-band region at R $\approx$ 37,000 with the Keck II telescope and the recently upgraded (Martin et al. 2018) Near-Infrared Spectrograph (NIRSpec; McLean et al. 1998) on 2019 April 8 (UT). Two rounds of A–B–B–A position nods were taken with individual exposure times of 150 s per nod position. The seeing was 0.″5–0.″6 overhead, though the target was observed at 1.8 airmasses. These data were processed using the REDSPEC package[12] and the resulting S/N = 60 at 1.08 μm.

5.2. Spectrum Characterization

Figures 5–11 illustrate some details of our spectra and are discussed in the subsections below, with the main features as follows. The Gaia 19ajj optical and infrared spectra exhibit many prominent lines that are indicative of outflowing material. There is evidence for both a neutral stellar/disk wind absorbing continuum radiation, and also shocked gas indicative of an outflowing jet. Weak metallic emission lines appear at the rest velocity.

In the optical, notably absent is strong photospheric absorption, with a few weak metallic lines identified, as discussed below. Several absorption features can be attributed to diffuse interstellar bands. In the infrared, the SXD observations in the *YJHK* bands indicate a red continuum with broad absorption due to molecular species. The LXD observations in the *L*-band exhibit a flat/blue continuum shape.

5.2.1. Wind Lines

Gaia 19ajj exhibits classic P Cygni structure in the Balmer Hα feature, with redshifted emission peaking around

[12] Written by L. Prato, S.S. Kim, & I.S. McLean.

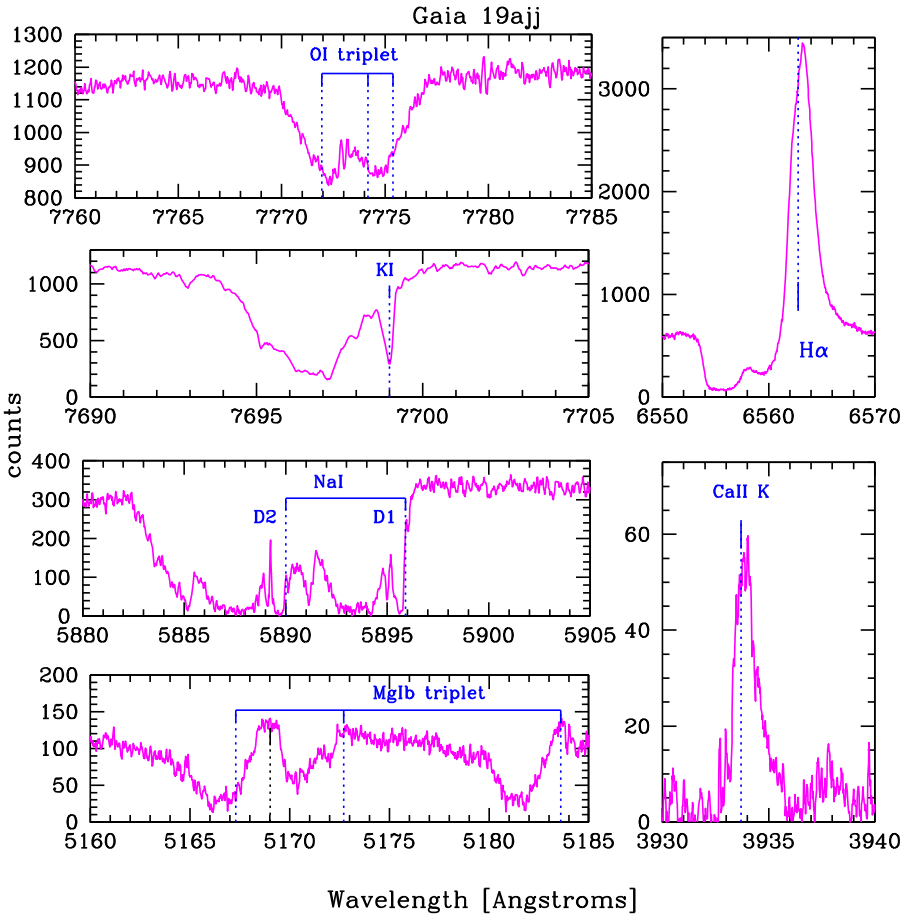

Figure 6. Portions of the Keck/HIRES spectrum illustrating the strong wind of Gaia 19ajj via blueshifted absorption features. The Hα profile has a clear P Cygni nature, extending to about -450 km s^{-1} on the blue side, with the red peak at $+25$ km s^{-1}. The Ca II K line may have a similar P Cygni profile, but the signal is low near the continuum level. Blueshifted absorption is also seen in the Mg I b triplet lines (with the bluest line contaminated by blueshifted Fe II 5169 Å), the Na I D doublet lines, the K I doublet, and the O I triplet—all signatures of a strong wind.

$+25$ km s^{-1} and blueshifted absorption extending to -450 km s^{-1} (Figure 6). Similar structure is seen more weakly in the infrared in the Paβ, Paγ, and Paδ lines, albeit from much lower spectral resolution (Figure 5). At Brγ there is simple emission, and Brδ and Br10 are in absorption, with very weak absorption or no sign of higher Br lines.

There is also a P Cygni signature in the Ca II infrared triplet lines around 8500 Å (Figure 5), which is likely present as well in the Ca II K line at 3933 Å (though masked by low S/N; Figure 6). Other lines with wind signatures in the form of purely blueshifted absorption include: Fe II 5018, 5169, and 5316, the Mg I b triplet, the Na I D doublet, the K I 7665/7699 doublet, the O I 7774 triplet (Figure 6), and the higher excitation He I 10830 triplet (Figures 5 and 11).

The hot He I line is very strong, reaching 50% of the continuum level in the earlier SpeX spectrum and all the way to 5% of the continuum in the later NIRSPEC spectrum, with the terminal velocity around -450 km s^{-1}. This assumes that the rest velocity is at a heliocentric velocity of $+35.8$ km s^{-1} which was the optical correction based on the Li I line, and indeed matches the location of the photospheric Mg II + Sr II line in the 1 μm spectrum. There is no signature of a feature in either absorption or emission at He I 5876 Å, which is the next transition higher from the 10830 Å upper level, and is optically thin. The wind models of Kwan et al. (2007) which treat the He I 10830 line formation as a purely scattering process from the continuum photons are consistent with our observations. More specifically, the breadth and depth of the Gaia 19ajj line profile (Figure 11) seem to match the genre of Kwan et al. (2007) models that adopt a stellar wind geometry rather than an inner disk wind geometry. Empirically, the He I profile of Gaia 19ajj most resembles that of the strong outflow source SVS 13, as illustrated in Edwards et al. (2006).

5.2.2. Jet Lines

Shocked outflowing gas is evidenced by blueshifted and broad emission in the optical doublets of [O I], [S II], [Ca II], [Fe II], and [Ni II]. As illustrated in Figure 7, all of these lines are double-peaked with the [S II] triply peaked. In most species the higher velocity component is stronger, but in [Ca II] the lower velocity component is stronger. Uniquely for the [Ca II] doublet lines, the low-velocity peak is at zero velocity relative to the star.

In the infrared (Figure 5), jet signatures manifest in several lines of [Fe II], along with shocked H_2 emission in the lowest energy lines. The O I line at 1.13 μm is somewhat broad, and has been associated with jets in other young sources.

The [Ca II], [Ni II], [Fe II], and [S II] lines exhibited in the optical and infrared spectra of Gaia 19ajj have intermediate ionization potential, 6.1–10.4 eV. There is no evidence of the often-seen lines of [O II] or [N II] which have higher ionization (13.6–14.5 eV), suggesting moderately low temperature. The

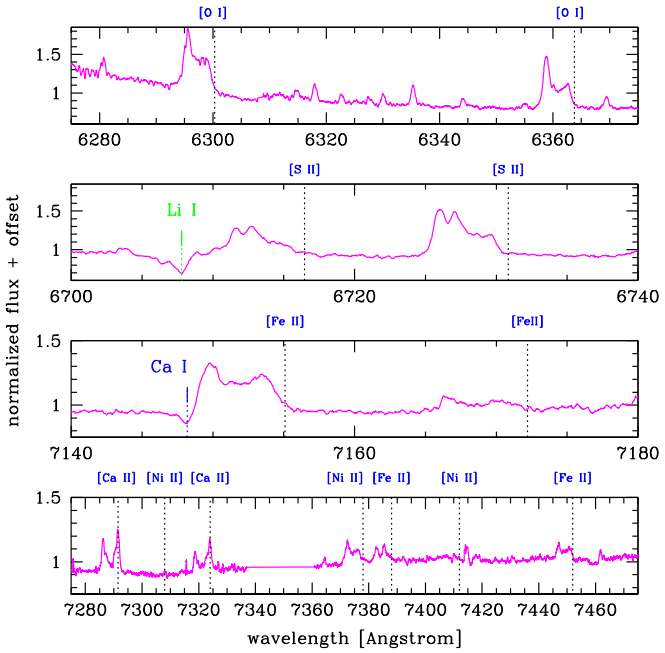

Figure 7. Portions of the Keck/HIRES spectrum illustrating the blueshifted forbidden emission lines, indicative of the presence of shocked gas in an outflowing jet. Note that the wavelength range differs among the panels. All species have multiply peaked profiles, with only the [Ca II] lines having an emission component at the rest velocity. Gaia 19ajj also exhibits clear Li I 6707 Å absorption.

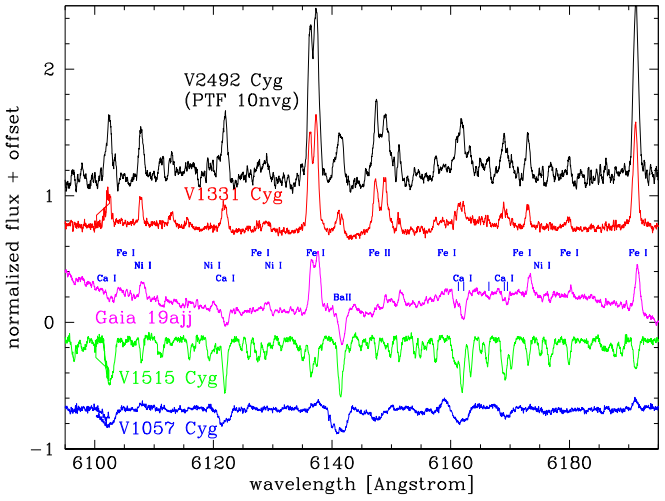

Figure 8. Portion of the HIRES spectrum highlighting the narrow emission lines and the weak absorption component of Gaia 19ajj. The emission series is similar to, but less extreme than the spectra exhibited by V2492 Cyg in its bright state (an object with a rather similar, large-amplitude lightcurve) and by V1331 Cyg, which is a well-known accretion-dominated object with a stochastic but relatively constant lightcurve (varying within 0.5 mag) over time. The absorption-dominated FU Ori stars V1515 Cyg and V1057 Cyg are also shown for comparison. There is little rest-velocity absorption in Gaia 19ajj, with this order unusually rich in such lines (labeled Ca I and Ba II, all of which are also present in the FU Ori stars).

various ratios among same species lines appear consistent with intermediate density ($>10^4$–6×10^5 cm^{-3})—except for the [Ca II].

The [Ca II] lines are high density (Ferland & Persson 1989; Hartigan et al. 2004; Nisini et al. 2005) and are unusual in T Tauri stars, even those showing the forbidden lines discussed above. They have been observed, however, in a number of

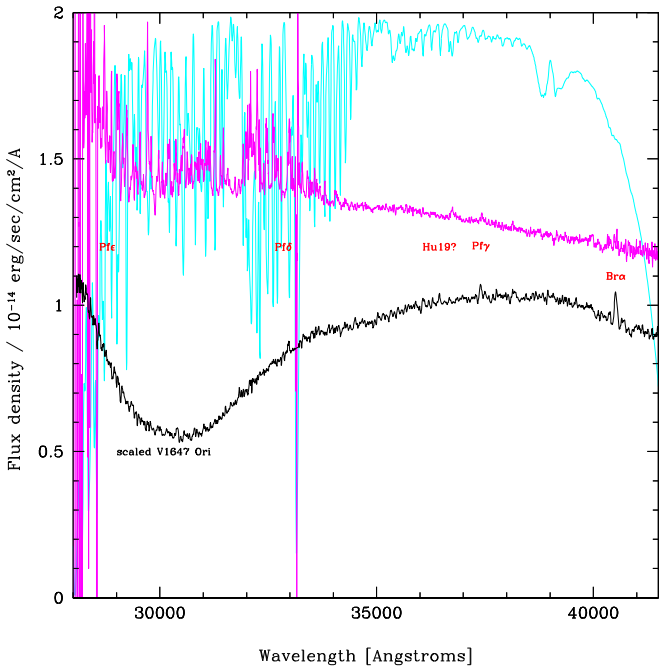

Figure 9. Long wavelength spectrum of Gaia 19ajj (magenta) compared to the Class I type variable V1647 Ori (black), which exhibits prominent broad absorption due to water ice. In contrast, the Gaia 19ajj continuum is slightly blue. Note that we attribute the apparent narrow emission in Gaia 19ajj throughout the water region to inaccurate telluric correction (cyan is a scaled atmospheric transmission spectrum). Weak hydrogen line emission is present in both sources.

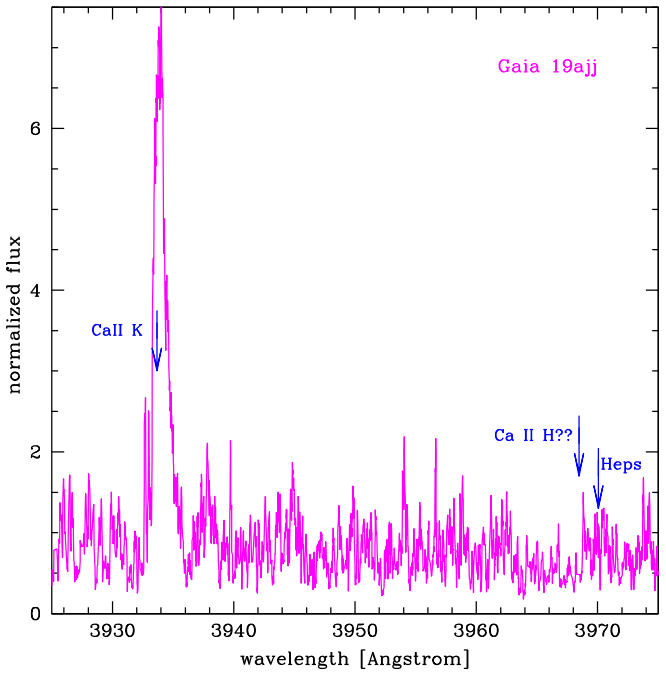

Figure 10. Ca II H and K spectral region, which is somewhat noisy but shows strong K yet no signature of H. These lines are a resonance doublet, and typically exhibit a K:H ratio of 1–2 in young stars. The ratio is significantly higher in Gaia 19ajj.

unusual large-amplitude photometric variables such as RW Aur, V2492 Cyg (PTF 10nvg), and PTF 14jg (Hillenbrand et al. 2019), as well as in the extreme emission-line young star V1331 Cyg. As mentioned above, the [Ca II] is the only

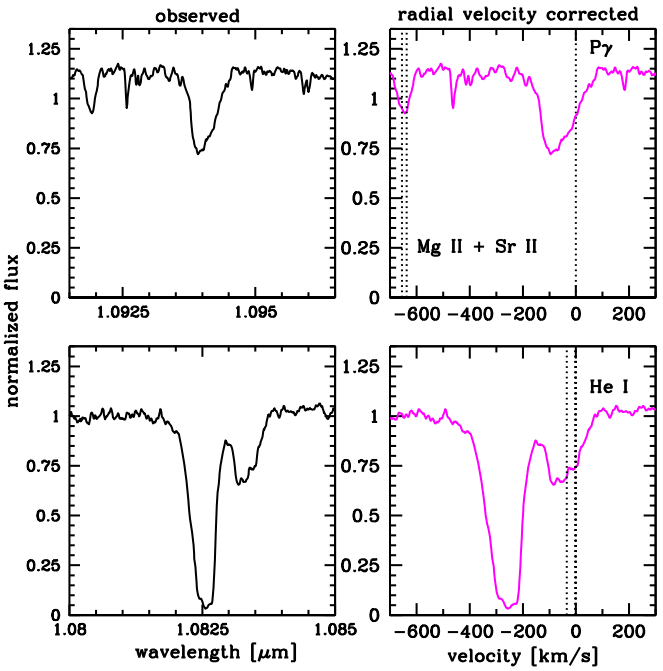

Figure 11. Portions of the Keck/NIRSPEC spectrum around He I 10830 Å and H I 10938 Å (Paγ), illustrating the blueshifted absorption in these lines (see the lower resolution data of Figure 5). The narrow features in the Paγ region are uncorrected telluric lines. Left panels are observed. Right panels are shifted by the same velocity as applied to the optical spectrum, resulting in excellent alignment for a narrow photospheric blend, thus confirming the inferred radial velocity. The hot He I gas is demonstrated to be outflowing with significant occultation of the 1 μm continuum by the outflow region. These line profiles can be compared to those exhibited by the cooler optical wind lines of Figure 6.

forbidden species in Gaia 19ajj having a zero-velocity component (Figure 7). The ratio of the 7291 Å to the 7324 Å is approximately 1.2:1, slightly lower than the expected 1.5:1 discussed in great detail by Hartigan et al. (2004). The [Ca II] lines are ground state transitions with their upper level populated either by collisions upward, or by downward transitions via the permitted Ca II triplet lines. If the [Ca II] occurs by fluorescence rather than collisions, this may explain both the different morphology relative to the other forbidden lines, and the slightly low doublet ratio.

5.2.3. Narrow Emission and Weak H I Emission Lines

There is narrow rest-velocity emission in Gaia 19ajj in permitted metallic lines such as Fe I, and Ni I in the optical, as illustrated in Figure 8. There is also weak metal emission in the infrared, as illustrated in Figure 5, which shows these same species plus other lines such as Mg I and Si I in *J*-band and *H*-band, and Na I in *K*-band. The line strengths are generally only $W_\lambda \gtrsim -1.0$ Å. This narrow emission spectrum is similar to that of the pre-peak spectrum of the FU Ori candidate outbursting source PTF 14jg (Hillenbrand et al. 2019), the large-amplitude accretion+extinction source V2492 Cyg (PTF 10nvg; Hillenbrand et al. 2013), as well as that of the photometrically quiet but extreme emission-line star V1331 Cyg.

The infrared spectrum of Gaia 19ajj also shows weak emission in the CO bandheads, though perhaps superposed on troughs of absorption (see the discussion below).

In the long wavelength spectrum (Figure 9), there is weak H I emission as evidenced by Brα, Pfγ, and Pfδ. There is another weak line at 3.675 μm that we cannot identify (the wavelength seems incorrect for Hu19 at 3.645 μm and there is no corresponding Hu18 at 3.693 μm). The spectrum bears some resemblance in showing these weak lines to V1647 Ori and Z CMa (Connelley & Reipurth 2018).

5.2.4. Interpreting the Strong Emission Lines

The strongest emission in Gaia 19ajj comes from Hα and Ca II, both associated with the accretion flow in typical young stars when these lines are strong and broad. The Hα line has $W_\lambda \approx -11$ Å in its redshifted emission component, but as discussed above there is also a strong blueshifted absorption component ($W_\lambda \approx 5$ Å) to the overall P Cygni type profile, weakening the emission strength. The 8542 Å line, usually the strongest of the Ca II triplet lines, has $W_\lambda = -6.3$ Å (integrated flux 4×10^{-14} erg s^{-1} cm^{-2} Å^{-1}), while the 3933 Å K line, usually the stronger of the Ca II doublet, has $W_\lambda \approx -18$ Å (with large uncertainty due to the low S/N in the continuum in this region). Again, there is likely blueshifted absorption in the Ca II lines that reduces the emission strengths.

We note with some interest the complete absence of the 3968 Å H line (see Figure 10), which is highly unusual given the generally comparable fluxes of the two components of the doublet (K:H ratio in the range 1–2) in most young accretors (e.g., Herczeg & Hillenbrand 2008; Rigliaco et al. 2012). In active chromospheres the K:H ratio increases as the activity level decreases and also occupies the range 1–2 (Houdebine & Stempels 1997). Suppression of the H line relative to the K line is clear in Gaia 19ajj and seems to defy the atomic physics prediction of a maximum ratio of 2 (in the optically thin case from the $g-f$ values). Despite the doublet ratio oddity, the three lines of the Ca II triplet, which share upper levels with the Ca II doublet, have typical ratios for young star accretors, around 0.95:1:0.85 for the 8498:8542:8662 Å lines. The usual interpretation is that the triplet lines are very optically thick (see the expected 0.11:1:0.55 proportions for optically thin lines).

An explanation for the peculiar doublet ratio is that there is contaminating P Cygni structure from Hε just 121 km s^{-1} redward of the Ca II H line. However, while Hα is strong in Gaia 19ajj, the upper Balmer lines are weak with only hints of Hγ, Hδ, and Hε. A complete cancellation of Ca II H emission having a strength of ∼50%–100% of the Ca II K line would require a coincidental Hε blueshifted absorption component of equal or larger strength, but without a redshifted emission component that exceeds the very weak Hε signal illustrated in Figure 10. We find that Herbig (1989) called attention to the same peculiarity of a lack of Ca II H despite strong Ca II K in the pre-outburst spectrum of V1057 Cyg, as well as noting it in FU Ori in the post-outburst state along with a few other unusual young stellar objects. The H line suppression may be a feature of sources with strong winds having a certain temperature and column density or optical depth.

5.2.5. The Photosphere

Gaia 19ajj is compared in Figure 5 to the FU Ori type star V1057 Cyg, which shows rather prominent ^{12}CO absorption in the 2.3 μm region (Connelley & Reipurth 2018; though weakening recently). As noted above, Gaia 19ajj shows some signatures of emission near the bandhead regions, which turn into a drop in the continuum toward redder wavelengths due to

the blended CO lines. The peculiarity of the CO region aside, there is resemblance of the Gaia 19ajj near-infrared spectrum with that of FU Ori stars in the prominent H_2O absorption feature, which is seen in all of the *K*-band, *H*-band, and *J*-bands (Connelley & Reipurth 2018). We have two SpeX spectra taken two months apart, and they show subtle but significant changes in the overall spectrum. Specifically in this interval, the water vapor absorption bands grew stronger, resulting in a more triangular shape through the *H*-band. At the same time, the CO emission lines in the *K*-band became slightly weaker, while the Brγ and the H_2 emission lines became slightly stronger. At longer wavelengths, Figure 9 shows only a flat continuum. There is no broad absorption between 2.8 and 3.3 μm due to water ice, as is seen in many young embedded or Class I type stars (e.g., Connelley & Reipurth 2018).

In terms of narrow atomic absorption, the low-resolution near-infrared spectrum of Gaia 19ajj exhibits little of the absorption due to atomic lines expected in an FU Ori interpretation. Our NIRSPEC spectrum, however, does show a photospheric line (Figure 11) that can be attributed to Sr II and/or Mg II, both intermediate ionization species. Wallace et al. (2000) demonstrate that this feature is prominent in F- and G-type supergiants, weaker in giants, and absent in dwarfs. In the optical, aside from the hallmark Li I 6707 Å youth signature (Figure 7), the strongest rest-velocity absorption that we have identified comes from Ca I and Ba II (Figure 8). Another order contains both Ca I 5857.45 and Ba II 5853.67. It is unclear why only Ca I absorption is strongly present, and not other lines having similar excitation. One clue may be that these lines have some surface gravity sensitivity for spectral types later than mid-G (Prisinzano et al. 2012). Besides these more obvious lines, only hints of weak absorption from other neutral metals appear in the Gaia 19ajj high resolution spectrum, especially in the 5500–5900 Å region, for example species such as Si, Sc, Mg, and Fe, Ni.

Regarding Ba II, the strongest (though blended) Ba II feature at 6497 Å unfortunately is between spectral orders in our HIRES spectrum. The illustrated 6142 Å line has $W_\lambda = 0.39$ Å, while the 5853 Å line has $W_\lambda = 0.16$ Å. These equivalent widths are notably stronger than the Ba II line strengths of normal dwarf stellar photospheres (of any spectral type). These lines are known to have a positive luminosity effect, and are strong in supergiants (Andrievsky 2006). The measured equivalent widths are about two-thirds of the line strengths seen in FU Ori, V1057 Cyg, and V1515 Cyg. While the Ba II line is typically seen in FU Ori sources, including in the recently announced objects *Gaia* 17bpi (Hillenbrand et al. 2018) and PTF 14jg (Hillenbrand et al. 2019); it is not present in other young stars. This is consistent with both the disk atmosphere (Hartmann & Kenyon 1985) and the distended stellar photosphere (Petrov & Herbig 1992) interpretation of the optical spectra of FU Ori objects, each of which are expected to produce low surface gravity spectral signatures.

6. Summary of Findings and Discussion

The source Gaia 19ajj recently exhibited a large-amplitude, long-term brightening event, rising in the optical by more than 5.5 mag over the past three years including over 3.5 mag in the past year. The body of evidence suggests that the source is a young star associated with a little-studied small dark cloud located behind the Gum Nebula. The source appears to have been comparably bright about 7 yr ago. Its recent color and magnitude behavior in the time domain suggest that variable extinction is part of the explanation for the slow undulative variations in the lightcurve during its overall large-amplitude rise. However, episodic accretion likely also plays a role since the lightcurve and color-curve data is inconsistent with pure extinction clearing. Furthermore, in its current bright state, the optical and infrared spectra of Gaia 19ajj exhibit strong accretion and outflow signatures. Similar to the early outburst stages of several categories of eruptive young stars, the strong wind has a rather high terminal velocity.

Some of the spectroscopic characteristics of Gaia 19ajj are FU Ori-like in nature. FU Ori stars are accretion outbursts, exhibiting large-amplitude photometric rises over months to years, with decay times of decades to centuries. Similarities include: mild water absorption in the near-infrared, rest-velocity Ba II and Li I in the optical, and strongly blueshifted, prominent absorption in several metal lines, indicative of a strong wind. The terminal wind velocity is higher in Gaia 19ajj than in many FU Ori stars, but objects such as V1735 Cyg, Z CMa, Par 21, and V582 Aur, as well as V1647 Ori (see below), do have comparable or even larger velocities. Absent from the Gaia 19ajj spectrum, at least in its present state, are the broad atomic photospheric absorption features and the obvious spectral type change with wavelength that are typical defining characteristics of FU Ori stars. The lightcurve is also unlike that of an FU Ori, showing a previous bright phase and substantial structure in the recent photometric rise.

Some spectrosopic characteristics of Gaia 19ajj are more like those of EX Lup-type accretion bursts. EX Lup stars exhibit distinct moderate-amplitude phototometric rises over weeks to months, with decay times of months. Notably in common is the narrow atomic emission seen in both the optical and the infrared (Kóspál et al. 2011; Sicilia-Aguilar et al. 2012), with the Gaia 19ajj narrow emission somewhat weaker than generally seen in EX Lup stars. EX Lup sources lack the strong wind signatures (clear P Cygni profiles with subcontinuum blueshifted absorption) of the FU Ori stars and exhibited by Gaia 19ajj.

Finally, some of Gaia 19ajj's spectroscopic characteristics are peculiar for either of the above outburst classes, notably the strong forbidden line emission.

We thus look beyond these popular categories of young star brightening and develop an analogy of Gaia 19ajj to sources that have been interpreted as accretion brightening combined with a reduction in the line-of-sight extinction along the path through the circumstellar envelope to the central young accretion system.

There are many well-known young stars that experience long-duration fades and recoveries relative to a fairly steady photometric baseline. Examples include GM Cep (e.g., Huang et al. 2019), V350 Cep (e.g., Semkov et al. 2017), and RW Aur (e.g., Koutoulaki et al. 2019), several of which exhibit UX Ori type behavior (photometric dimming events that are accompanied by reddening which turns blueward near the depths of the fades). The photometric excursions of these objects are lower amplitude than seen in the lightcurve of Gaia 19ajj, and they do not seem to exhibit signs of enhanced accretion during the bright phases.[13] A star with a lightcurve more like that of Gaia 19ajj is HBC 340 (Dahm & Hillenbrand 2017), which also exhibits an undulating photometric rise but, like the

[13] Although this has been claimed photometrically for GM Cep, the spectroscopy of Giannini et al. (2018) indicates otherwise.

sources mentioned above, does not have an accompanying enhancement in the spectroscopic accretion/wind indicators.

V2492 Cyg has been characterized as a star with large-amplitude magnitude and color variations, a manifestation of extinction variations, but perhaps ultimately driven by accretion variations (see, e.g., Covey et al. 2011; Hillenbrand et al. 2013; Kóspál et al. 2013; Giannini et al. 2018). A notable aspect of this source is that, in its faint state, the spectrum of V2492 Cyg is dominated by forbidden line emission formed in the jet/outflow (which becomes stronger than Hα as the source fades). The bright state, by contrast, features mostly lines that are formed in the magnetospheric infall region or the accretion shock. Gaia 19ajj's bright state spectrum is not as strong or quite as rich in emission lines as V2492 Cyg, but there are definite spectral similarities (e.g., Figure 8). However, V2492 Cyg does not exhibit the molecular absorption in H_2O nor the possible CO region absorption that Gaia 19ajj shows (e.g., Figure 5). We also note that there is no Ba II signature in V2492 Cyg.

PV Cep is another source with large-amplitude photometric variations and also an emission-line-dominated spectrum with no or very weak absorption in the optical. Over the past decade, this source experienced a ≈3 mag unsteady rise over about 5 yr,[14] quite similar in timescale to Gaia 19ajj though not as large in amplitude, and similar in amplitude to V2492 Cyg but with a shorter timescale. Before this, it had experienced a flux decrease of ≈4 mag accompanied by a weakening of the robust Ca II triplet emission accretion indicator (Kun et al. 2011). The behavior was attributed to a combination of reduced accretion and enhanced extinction effects, the latter possibly related to changes in the inner disk structure. Lorenzetti et al. (2011) discusses the optical and infrared photometric variations of PV Cep. Caratti o Garatti et al. (2013) discuss the infrared emission-line spectrum, which is much stronger than that of Gaia 19ajj, including clear CO bandhead emission and stronger jet lines (e.g., [Fe II] and H_2). Despite the stronger emission, the wind signatures of PV Cep appear not as prevalent as they are in Gaia 19ajj. It remains an interesting analog, however.

Comparison can also be made to V1647 Ori, which is a repeating burst source that is sometimes associated with the EX Lup category, but has larger amplitude, longer duration, and less frequent bursts than most EX Lup stars; it is perhaps best characterized as being the prototype of the V1647 Ori category. As for V2492 Cyg, while there are large color changes in V1647 Ori, extinction variations are not the dominant effect on the lightcurve (e.g., McGehee et al. 2004; Acosta-Pulido et al. 2007; Aspin & Reipurth 2009). Further, the permitted emission lines in this source are even stronger than in V2492 Cyg or Gaia 19ajj, and there was only weak forbidden emission during the V1647 Ori outbursts. There is also no Ba II signature in V1647 Ori.

7. Conclusion

While it is often tempting for authors to categorize large-amplitude photometric variability in young stars in terms of known families, the variability phase space is still rather incompletely mapped. On timescales of weeks to months, there are clear differences between the variability types exhibited by Class I sources relative to those in later stages of circumstellar evolution (Class II and Class III sources), with Class I variability tending to be larger amplitude and longer timescale (Rebull et al. 2015; Wolk et al. 2018). Over months to years, both the Class I and the Class II sources can show long duration trends, as well as distinct episodic brightening events that last months to decades.

Gaia 19ajj is an example of a Class I object that is clearly a rapid accretor and driving a strong outflow. The recent photometric brightening is indeed likely driven in large part by a positive change in the accretion/outflow activity, which has also caused a reduction in the line-of-sight extinction to the central star and inner accretion zone. Although Gaia 19ajj exhibits some FU Ori-like absorption characteristics in its spectrum, notably Ba II in the optical, as well as several other low-gravity atomic lines, and broad molecular absorption in the near-infrared, it also displays EX Lup-like emission (in both the optical and the near-infrared *J*-band). We conclude that the best analogs may be V2492 Cyg, PV Cep, and possibly V1647 Ori, in which there are substantial changes in extinction that accompany enhanced accretion. All of these objects appear to have a repeating brightening and fading pattern on timescales of several years. It is not yet obvious to which, if any, of the above variable-accretion categories Gaia 19ajj should be associated.

We gratefully acknowledge Simon Hodgkin for his stewardship of the *Gaia* Photometric Science Alerts, as well as the *Gaia* Photometric Science Alerts Team, DPAC, and ESA/*Gaia*. We also gratefully acknowledge the NASA/NEOWISE Team. Andrew Howard enabled the Keck/HIRES data acquisition. Trevor David investigated for us the potential availability of *TESS* data. This research has made extensive use of CDS services such as SIMBAD and Vizier. This research has benefited from consultation of the AAVSO Database; we acknowledge with thanks the variable star observations contributed there by observers worldwide. Finally, we are grateful to the referee for a detailed review of our work.

Facilities: Gaia, ASAS-SN, IRTF:SpeX, Keck:I (HIRES), Keck:II (NIRSPEC), 2MASS, *WISE*, NEOWISE, IRSA.

ORCID iDs

Bo Reipurth https://orcid.org/0000-0001-8174-1932
Michael Connelley https://orcid.org/0000-0002-8293-1428
Roc M. Cutri https://orcid.org/0000-0002-0077-2305
Howard Isaacson https://orcid.org/0000-0002-0531-1073

References

Acosta-Pulido, J. A., Kun, M., Ábrahám, P., et al. 2007, AJ, 133, 2020
Ambartsumian, V. A. 1949, AZh, 26, 3
Andrievsky, S. M. 2006, AN, 319, 239
Aspin, C., & Reipurth, B. 2009, AJ, 138, 1137
Barentsen, G., Farnhill, H. J., Drew, J. E., et al. 2014, MNRAS, 444, 3230
Barentsen, G., Vink, J. S., Drew, J. E., & Sale, S. E. 2013, MNRAS, 429, 1981
Bhatt, H. C., Jain, S. K., & Sagar, R. 1998, A&A, 331, 737
Caratti o Garatti, A., Garcia Lopez, R., Weigelt, G., et al. 2013, A&A, 554, A66
Cody, A. M., & Hillenbrand, L. A. 2018, AJ, 156, 71
Cody, A. M., Stauffer, J., Baglin, A., et al. 2014, AJ, 147, 82
Connelley, M. S., & Reipurth, B. 2018, ApJ, 861, A145
Connelley, M. S., Reipurth, B., & Tokunaga, A. T. 2007, AJ, 133, 1528
Contreras Peña, C., Naylor, T., & Morrell, S. 2019, MNRAS, 486, 4590
Covey, K. R., Hillenbrand, L. A., Miller, A. A., et al. 2011, AJ, 141, A40
Cushing, M. C., Rayner, J. T., & Vacca, W. D. 2005, ApJ, 623, 1115
Cushing, M. C., Vacca, W. D., & Rayner, J. T. 2004, PASP, 116, 362

[14] See, e.g., https://www.aavso.org.

Cutri, R. M., Mainzer, A., & Conrow, T. 2015, Explanatory Supplement to the NEOWISE Data Release Products, http://wise2.ipac.caltech.edu/docs/release/neowise/expsup
Cutri, R. M., Skrutskie, M. F., van Dyk, S., et al. 2003, 2MASS All SkyCatalog of Point Sources (Washington, DC: NASA)
Dahm, S. E., & Hillenbrand, L. A. 2017, AJ, 154, 177
Dobashi, K. 2011, PASJ, 63, S1
Drew, J. E., Gonzalez-Solares, E., Greimel, R., et al. 2014, MNRAS, 440, 2036
Dutra, C. M., & Bica, E. 2002, A&A, 383, 631
Edwards, S., Fischer, W., Hillenbrand, L., & Kwan, J. 2006, ApJ, 646, 319
Ferland, G. J., & Persson, S. E. 1989, ApJ, 347, 656
Gaia Collaboration, Brown, A. G. A., Vallenari, A., et al. 2018, A&A, 616, A1
Giannini, T., Munari, U., Antoniucci, S., et al. 2018, A&A, 611, A54
Giannini, T., Munari, U., Lorenzetti, D., et al. 2018, RNAAS, 2, 124
Gum, C. S. 1955, MmRAS, 67, 155
Hartigan, P., Edwards, S., & Pierson, R. 2004, ApJ, 609, 261
Hartley, M., Manchester, R. N., Smith, R. M., et al. 1986, A&AS, 63, 27
Hartmann, L., & Kenyon, S. J. 1985, ApJ, 299, 462
Hartmann, L., & Kenyon, S. J. 1996, ARA&A, 34, 207
Herbig, G. H. 1946, PASP, 58, 163
Herbig, G. H. 1954, JRASC, 46, 222
Herbig, G. H. 1957, in IAU Symp. 3, Non-Stable Stars, ed. G. H. Herbig (Cambridge: Cambridge Univ. Press), 3
Herbig, G. H. 1977, ApJ, 217, 693
Herbig, G. H. 1989, in European Southern Observatory Conf. and Workshop Proc. 33, ed. B. Reipurth (Garching: ESO), 233
Herbst, W., Herbst, D. K., Grossman, E. J., et al. 1994, AJ, 108, 1906
Herbst, W., & Shevchenko, V. S. 1999, AJ, 118, 1043
Herczeg, G. J., & Hillenbrand, L. A. 2008, ApJ, 681, 594
Hillenbrand, L. A., Contreras Peña, C., Morrell, S., et al. 2018, ApJ, 869, A146
Hillenbrand, L. A., & Findeisen, K. P. 2015, ApJ, 808, 68
Hillenbrand, L. A., Miller, A. A., Carpenter, J. M., et al. 2019, ApJ, 874, 82
Hillenbrand, L. A., Miller, A. A., Covey, K. R., et al. 2013, AJ, 145, 59
Hodgkin, S. T., Wyrzykowski, L., Blagorodnova, N., & Koposov, S. 2013, RSPTA, 371, 20120239
Houdebine, E. R., & Stempels, H. C. 1997, A&A, 326, 1143
Howard, A. W., Marcy, G. W., Johnson, J. A., et al. 2010, Sci, 330, 653
Huang, P. C., Chen, W. P., Mugrauer, M., et al. 2019, ApJ, 871, A183
Ibryamov, S. I., Semkov, E. H., & Peneva, S. P. 2015, PASA, 32, e021
Indebetouw, R., Mathis, J. S., Babler, B. L., et al. 2005, ApJ, 619, 931
Ishihara, D., Onaka, T., Kataza, H., et al. 2010, A&A, 514, A1
Ismailov, N. Z. 2005, ARep, 49, 309
Joy, A. H. 1945, ApJ, 102, 168
Kóspál, Á, Ábrahám, P., Acosta-Pulido, J. A., et al. 2013, A&A, 551, A62
Kóspál, Á, Ábrahám, P., Goto, M., et al. 2011, ApJ, 736, 72
Koutoulaki, M., Facchini, S., Manara, C. F., et al. 2019, A&A, 625, A49
Krisciunas, K., Sinton, W., Tholen, K., et al. 1987, PASP, 99, 887
Kun, M., Szegedi-Elek, E., Moór, A., et al. 2011, MNRAS, 413, 2689
Kwan, J., Edwards, S., & Fischer, W. 2007, ApJ, 657, 897
Lorenzetti, D., Giannini, T., Larionov, V. M., et al. 2011, ApJ, 732, 69
Maehara, H., Kojima, T., & Fujii, M. 2014, ATel, 6770, 1
Mainzer, A., Bauer, J., Cutri, R. M., et al. 2014, ApJ, 792, A30
Martin, E. C., Fitzgerald, M. P., McLean, I. S., et al. 2018, Proc. SPIE, 10702, 107020A
Marton, G., Tóth, L. V., Paladini, R., et al. 2016, MNRAS, 458, 3479
May, J., Murphy, D. C., & Thaddeus, P. 1988, A&AS, 73, 51
McGehee, P. M., Smith, J. A., Henden, A. A., et al. 2004, ApJ, 616, 1058
McLean, I. S., Becklin, E. E., Bendiksen, O., et al. 1998, Proc. SPIE, 3354, 566
Monet, D. 1998, USNO-A2.0 (Flagstaff, AZ: U.S. Naval Observatory)
Monet, D. G., Levine, S. E., Canzian, B., et al. 2003, AJ, 125, 984
Mutafov, A. S., Semkov, E. H., Ibryamov, S. I., & Peneva, S. P. 2019, AIPC, 2075, 090004
Nisini, B., Bacciotti, F., Giannini, T., et al. 2005, A&A, 441, 159
Parker, Q. A., Phillips, S., Pierce, M. J., et al. 2005, MNRAS, 362, 689
Petrov, P. P., & Herbig, G. H. 1992, ApJ, 392, 209
Pettersson, B. 1987a, A&A, 171, 101
Pettersson, B. 1987b, A&AS, 70, 69
Planck Collaboration, Ade, P. A. R., Aghanim, N., et al. 2011, yCat, VIII, 88
Price, S. D., Egan, M. P., Carey, S. J., Mizuno, D. R., & Kuchar, T. A. 2001, AJ, 121, 2819
Prisinzano, L., Micela, G., Sciortino, S., Affer, L., & Damiani, F. 2012, A&A, 546, A9
Rayner, J. T., Toomey, D. W., Onaka, P. M., et al. 2003, PASP, 115, 362
Rebull, L. M., Stauffer, J. R., Cody, A. M., et al. 2015, AJ, 150, 175
Reipurth, B. 1983, A&A, 117, 183
Reipurth, B., & Aspin, C. 2010, in Proceedings of the Conference dedicatedto Viktor Ambartsumian's 100th anniversary: Evolution of Cosmic Objects through their Physical Activity, ed. H. A. Harutyunian, A. M. Mickaelian, & Y. Terzian (Yerevan: Publishing House of NAS RA), 19
Reipurth, B., Aspin, C., & Herbig, G. H. 2012, ApJL, 748, L5
Rigliaco, E., Natta, A., Testi, L., et al. 2012, A&A, 548, A56
Rodgers, A. W., Campbell, C. T., & Whiteoak, J. B. 1960, MNRAS, 121, 103
Schlafly, E. F., Green, G. M., Lang, D., et al. 2018, ApJS, 234, 39
Semkov, E. H., Ibryamov, S. I., & Peneva, S. P. 2017, BlgAJ, 27, 75
Shappee, B. J., Prieto, J. L., Grupe, D., et al. 2014, ApJ, 788, A48
Sicilia-Aguilar, A., Kóspál, Á, Setiawan, J., et al. 2012, A&A, 544, A93
Simons, D. A., & Tokunaga, A. 2002, PASP, 114, 169
Skrutskie, M. F., Cutri, R. M., Stiening, R., et al. 2006, AJ, 131, 1163
Vogt, S. S., Allen, S. L., Bigelow, B. C., et al. 1994, Proc. SPIE, 2198, 362
Wallace, L., Meyer, M. R., Hinkle, K., et al. 2000, ApJ, 535, 325
Westerlund, B. E. 1963, MNRAS, 127, 71
Wolk, S. J., Günther, H. M., Poppenhaeger, K., et al. 2018, AJ, 155, 9
Wright, E. L., Eisenhardt, P. R. M., Mainzer, A. K., et al. 2010, AJ, 140, 1868
Zacharias, N., Monet, D. G., Levine, S. E., et al. 2005, yCat, I, 297